

Structural Characterization and Corrosion Behavior of Stainless Steel Coated With Sol-Gel Titania

Daniela C.L. Vasconcelos, Eduardo H.M. Nunes, Antônio Claret S. Sabioni, João C. Diniz da Costa, and Wander L. Vasconcelos

(Submitted May 3, 2010; in revised form March 14, 2011)

Sol-gel titania films were prepared from hydrolysis and condensation of titanium (IV) isopropoxide. Diethanolamine was used as chelant agent in titania synthesis. 316L stainless steel substrates were dip-coated at three different withdrawal speeds (6, 30, and 60 mm/min) and heated up to 400 °C. Thermogravimetry and differential thermal analyses of the titania gel solution evinced a continuous mass loss for temperatures up to 800 °C. The transition of anatase to the rutile phase begins at 610–650 °C, being the rutile transformation completed at 900 °C. The thicknesses of the films were determined as a function of the heat treatment and withdrawal speed. It was observed that their thicknesses varied from 130 to 770 nm. Scanning electron microscopy images of the composites revealed the glass-like microstructure of the films. The obtained sol-gel films were also characterized by energy dispersive spectroscopy. The chemical evolution of the films as a function of the heating temperature was evaluated by Fourier transform infrared spectroscopy (specular reflectance method). After performing the adhesion tests, the adherence of the titania films to the stainless steel substrate was excellent, rated 5B according to ASTM 3359. The hardness of the ceramic films obtained was measured by the Knoop microindentation hardness test with a 10 g load. We observed that the titania film became harder than the steel substrate when it was heated above 400 °C. The corrosion rates of the titania/steel composites, determined from potentiodynamic curves, were two orders of magnitude lower than that of the bare stainless steel. The presence of the sol-gel titania film contributed to the increase of the corrosion potential in ca. 650 mV and the passivation potential in ca. 720 mV.

Keywords corrosion, sol-gel, steel, structural properties, titanium oxide

1. Introduction

Coating composites, or surface engineered materials, are designed specifically to improve properties such as optical, electrical, tribological, chemical, biological, among others (Ref 1). The sol-gel process is very attractive in coating technology owing to the good adhesion of sol-gel as it interfaces with solid surfaces. In addition, the sol-gel film formation requires considerably less equipment and is potentially less expensive than other techniques such as chemical vapor deposition (CVD), evaporation, or sputtering (Ref 2). Therefore, coating based on sol-gel processing has been extensively deployed for a myriad of application. Particularly,

Daniela C.L. Vasconcelos, Eduardo H.M. Nunes, and Wander L. Vasconcelos, Department of Metallurgical and Materials Engineering, Laboratory of Ceramic Materials, Federal University of Minas Gerais, Avenida Presidente Antônio Carlos, 6627, sala 2230, Pampulha, Campus UFMG, Escola de Engenharia, bloco 2, CEP 31270-901 Belo Horizonte, MG, Brazil; **Antônio Claret S. Sabioni**, Department of Physics, Federal University of Ouro Preto, CEP: 35400-000 Ouro Preto, MG, Brazil; and **João C. Diniz da Costa**, Films and Inorganic Membrane Laboratory, School of Chemical Engineering, The University of Queensland, FIMLab, Brisbane, QLD 4072, Australia. Contact e-mails: eduardohmn@yahoo.com.br and wlv@demet.ufmg.br.

this topic draws considerable attention from the research community as a method used to modify surface properties on a variety of substrates at relatively low temperatures (Ref 3–10).

The deposition parameters (sol composition, dip coating withdrawal speed) together with the substrate characteristics (composition, microstructure, and surface finish) determine coating and composite properties (thickness, chemical composition, microstructure, performance, etc.). In order to improve the corrosion resistance of metals by applying coatings, various sol-gel oxide films have been studied (Ref 11–16).

The use of polymers as protective coatings for steel against acid corrosion has been proposed by some researchers (Ref 17, 18). However, these materials cannot be exposed to high temperatures or aggressive environments (Ref 19, 20). According to Vasconcelos (Ref 21), metallic coatings present the same constraints.

Izumi et al. (Ref 22) reported an increase in chemical resistance of aluminized steel sheets coated with sol-gel silica and zirconia, in a 5% NaCl solution. Using tetraethylorthosilane as the start material, Vasconcelos et al. (Ref 23) obtained composite systems sol-gel silica/304 stainless steel with higher corrosion resistance in a 1 N H₂SO₄ and 3.5% NaCl medium. Based on Rutherford backscattering spectroscopy data, the authors concluded that the intermediate layer formed between the silica film and the steel substrate is responsible for the increase of the corrosion resistance of the stainless steel. Atik et al. (Ref 24) studied the corrosion improvement of 316 steel using titania-silica and alumina-silica sol-gel films. They observed that the coatings allowed a remarkable increase of the stainless steel lifetime when placed in a 3% NaCl solution. Titania (TiO₂) films have attracted attention as photoelectrode,

photocatalyst, gas sensor and biomaterial, when used for coating titanium alloys or 316L stainless steel.

As far as we know, the corrosion behavior of the composite system sol-gel titania film/316L stainless steel in a 1 N H₂SO₄ solution has not been explored yet. In this work, it was evaluated through the structural characterization of the composites produced.

2. Experimental Procedure

Prior to coating, to improve the adhesion of films on metal surfaces, the metal surface must be prepared. In the present work, the 316L stainless steel was cut in pieces of 3.0 × 3.0 cm, polished until 600 mesh to a higher surface finishing, washed with detergent, deionized water, and degreased with acetone. Finally, the sample was placed in an ultrasonic bath with acetone and dried in hot air.

The sol-gel titania solution was prepared hydrolyzing titanium tetraisopropoxide (Ti(OC₃H₇)₄) as described elsewhere (Ref 25). The molar ratios of precursor/ethanol and acetic acid/diethanolamine were 16 and 1, respectively. The as-prepared solution was deposited on the 316L stainless steel substrates by means of the dip-coating technique, using 6, 30, and 60 mm/min withdrawal speeds. The coated substrates were heat treated at 100, 300, and 400 °C in an open to air oven.

Self-supporting films were prepared by pouring the sol over a nonadherent surface for subsequent evaluation of their thermal behavior. Thermogravimetry (TGA) and differential thermal (DTA) analyses were conducted under nitrogen atmosphere, with a ramp rate of 10 °C/min (Shimadzu, TA-50). The density of the gels obtained in foil form was measured using He pycnometer (Quantachrome Corporation, Multipycnometer).

The thicknesses of the titania films were calculated from the deposited mass, and based on the density as measured by He pycnometry. The synthesized films were characterized by scanning electron microscopy (Phillips XL30) and energy dispersive spectroscopy (EDAX-DX4). The infrared spectra of the films were measured by Fourier transform infrared (FTIR) spectroscopy (Perkin Elmer, Paragon 1000) employing specular reflectance (SR) technique, with a spectral resolution of 4 cm⁻¹ and 32 scans for each spectrum. The adherence of titania films to the stainless steel substrate was measured after cross-cut tape adhesion tests. These tests were performed as described in ASTM D3359 (Ref 26). The film hardness was obtained with a microindentation hardness test, using Knoop indenter, with a dwell time of 15 s (Future Tech, FM-1). The bare stainless steel and the composites were submitted to accelerated corrosion tests, in 1 N H₂SO₄ deaerated solution, making use of a potentiostat-galvanostat (Radiometer-Copenhagen, VoltaMaster1). We used a nitrogen flow rate of 30 NL/h; the scanning velocity was 167 × 10⁻³ mV/s and the reference electrode was saturated calomel.

The chemical profile composition (varying from the surface toward the substrate) of the titania composite, was evaluated via glow discharge spectrometry—GDS (depth resolved, radio frequency glow discharge atomic emission spectrometry, with a Jobin-Yvon 5000RF). The elements analyzed in this work were Ti, O, Fe, Cr, Ni, Si, and Mn. The tested surface area of the samples was about 12.5 mm². For each sample, the time data has been converted to depth through the multiplication of the crater size by the average sputter rate.

3. Results and Discussion

3.1 Thermal Analysis

A typical TGA curve of a titania gel self-supporting film appears in Fig. 1, showing a total 57% mass loss for temperatures up to 1000 °C. Further investigation of these results by DTA analysis suggests that the mass loss ratio as a function of the temperature can be allocated to five distinct regions. The first region extends from room temperature up to 100 °C with a mass loss of 4.5%. There is an endothermic peak below 100 °C, which is ascribed to desorption of physically bonded water and alcohol from the film (Ref 27-29). Continuing from this temperature, the mass loss for the second region increases to 10.5% up to ca. 300 °C, which is attributed to elimination of organic groups related to the exothermic peak at 322 °C. At the third region, between 300 and 580 °C, the mass loss increases to 23%. The exothermic peak at 440 °C is associated with the beginning of anatase phase formation (Ref 29). Increasing temperature to the fourth region (580 and 780 °C) attracts further 19% mass loss. At this region, another exothermic peak appears about 640 °C ascribed to a second dehydroxylation of strongly bonded OH groups (Ref 30). In addition, transition of anatase to the rutile phase begins at 610-650 °C (Ref 31). The fifth and last region begins about 780 °C and is distinguished by the end of the mass loss of the titania gel self-supporting film. The rutile transformation is therefore completed at 900 °C (Ref 27), as observed by the last exothermic peak in Fig. 1.

3.2 Temperature Effects on Film Thickness

In order to determine film thickness using coating mass, it is necessary to know the coated volume of the sample and the film density. In this work, we poured the titania sol over a nonadherent surface obtaining some gel sheets resembling a nonsupported thin film. We observed that these films are mechanically flexible and can be bent very easily without causing film breakage. This is an important property, with potential application for coating metal parts of different shapes and sizes. The measured mean density of the titania films by He pycnometry was 1.75 ± 0.11 g/cm³.

Figure 2 shows the dependence between the estimated average thickness of the film formed on 316L steel surface as a function of the heat-treatment temperature under atmospheric conditions. We observed that the films become thinner for all three set of withdrawal velocities by raising the heat-treatment temperature. These results suggest that the film mass was reduced in accordance with the TGA results (Fig. 1). The most

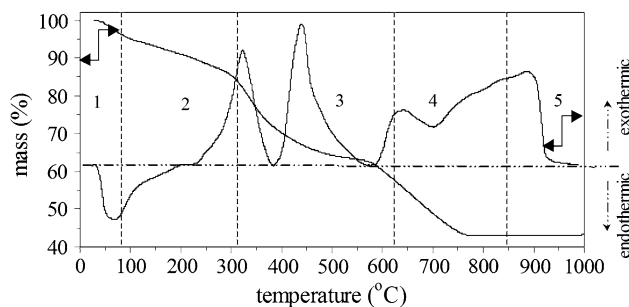


Fig. 1 TG and DTA curves of titania unsupported film

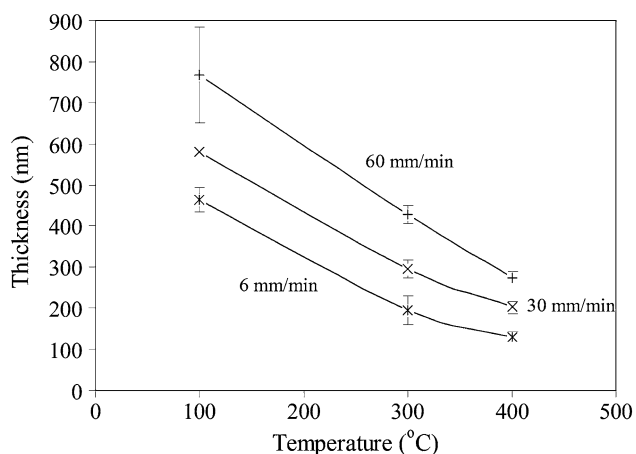


Fig. 2 Film thickness as a function of the temperature

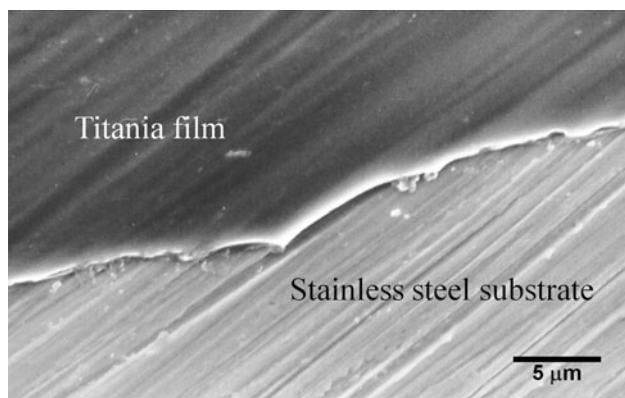


Fig. 3 SEM image of the sol-gel titania film/316L stainless steel composite heat treated at 300 °C

significant thickness reduction occurred between 100 and 300 °C and corresponds to a mean reduction of 50 (± 7)%. At this temperature range, the large organic groups are combusted, thus allowing for a higher rate of film densification. Between 300 and 400 °C, the additional reduction in average thickness was 17 (± 3)%. The dependence of the mass loss ratio (or thickness reduction) with the temperature for the film heated in an open to air oven was higher than the observed for the titania gel used in the TGA. It is important to remember that these analyses were performed under nitrogen atmosphere. Probably, this difference in the mass loss ratio is associated to the high amount of organic phases in the film, which can oxidize and be released at lower temperatures (Ref 27). Another parameter that may contribute to the high mass loss ratio of the film is its greater surface area.

3.3 Film Composition

A typical surface of the sol-gel titania film heat treated at 300 °C resulted in the formation of a shining vitreous surface. The SEM micrograph (Fig. 3) shows a homogeneous titania film without large precipitates, cracks, or peeling. The EDS analyses of the titania film/316L stainless steel composite revealed in addition to Ti and O, the presence of the elements that make up the substrate (Fe, Cr, Ni, Mn, Mo, and Si).

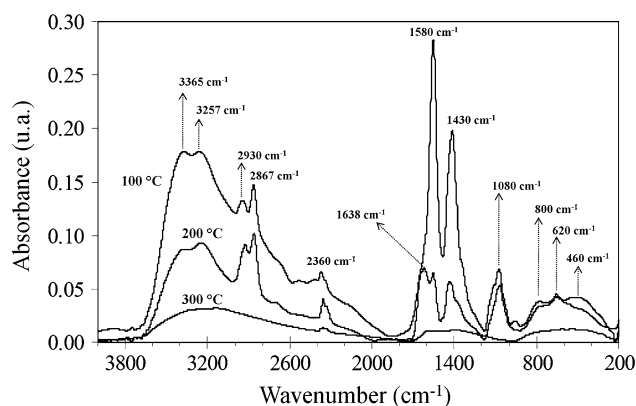


Fig. 4 FTIR spectra of sol-gel titania films heat treated at 100, 200, and 300 °C

Figure 4 shows SR-FTIR spectra of sol-gel titania films heat treated at 100, 200, and 300 °C. The broad absorption band centered at 3300 cm^{-1} is attributed to stretching vibrations of molecular water and OH groups (Ref 32). Superimposed onto this band, two other bands are clearly visible at 3365 and 3257 cm^{-1} . These two bands have been ascribed, respectively, to the asymmetric and symmetric stretching vibration of N-H groups from diethanolamine. Next to them there are two additional peaks at 2930 and 2867 cm^{-1} which correspond to the symmetric $\nu_s(\text{CH}_2)$ and asymmetric $\nu_{as}(\text{CH}_2)$ stretching vibrations from the alkoxide (Ref 33, 34). The bands near 2360 cm^{-1} are related to atmospheric CO_2 present in the instrument environment.

The absorption bands at 1580 and 1430 cm^{-1} are assigned, respectively, to the asymmetric $\nu_{as}(\text{COO})$ and symmetric $\nu_s(\text{COO})$ stretching vibrations. The separation of 150 cm^{-1} observed for the $\nu_{as}(\text{COO})$ and $\nu_s(\text{COO})$ peak positions is typical for bidentate-bridged carboxylic acid titanium complexes (Ref 35). According to Urlaub et al. (Ref 34) and Venz et al. (Ref 36), three coordination modes of carboxylic acids to a metal atom are possible, namely monodentate via one oxygen atom, bidentate chelating via both oxygen atoms, and bidentate bridging between two metal atoms.

The peak at 1638 cm^{-1} is due to the $\nu(\text{C}=\text{C})$ mode (Ref 34). The bands for Ti-O and Ti-O-Ti bonds are present in the 800-400 cm^{-1} region, the former being observed in a higher wavenumber than the latter (Ref 33, 37). One notices that the increase of the sample heating temperature leads to a decrease in the absorption intensities of OH groups (bands about 3200 cm^{-1}) and of organic groups (bands about 1440-1640 cm^{-1}) with respect to Ti-O and Ti-O-Ti bonds.

It is important to notice that even in films heated only up to 100 °C, the band about 1715 cm^{-1} , characteristic of the stretch vibration of the C=O bonds of free carboxylic acids, is absent. This excludes the presence of an ester group from the reaction of titanium isopropoxide with acetic acid in the sol-gel coating (Ref 34).

As mentioned before, the composition depth profile of the sol-gel titania films were evaluated by GDS. The intensities of O, Mn, and Si have been normalized for each sample by multiplying the signal by 10, 5, and 2, respectively, so that the profiles could be presented in the same scale. Figure 5 shows the chemical depth profile of the composites obtained from films deposited at a withdraw speed of 60 mm/min and heat treated at 400 °C. Since the depths on the graph are obtained

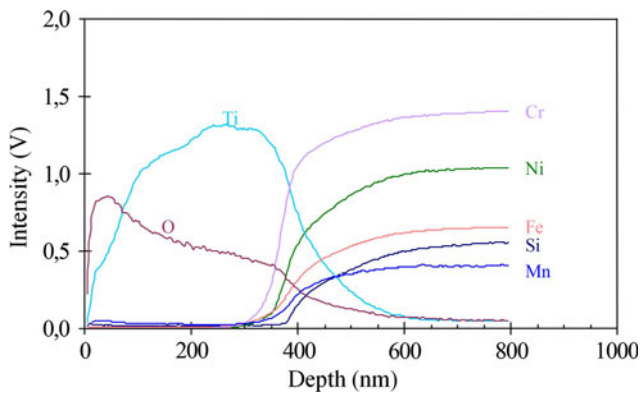


Fig. 5 GDS of a titania sol-gel film deposited at 60 mm/min and heated up to 400 °C

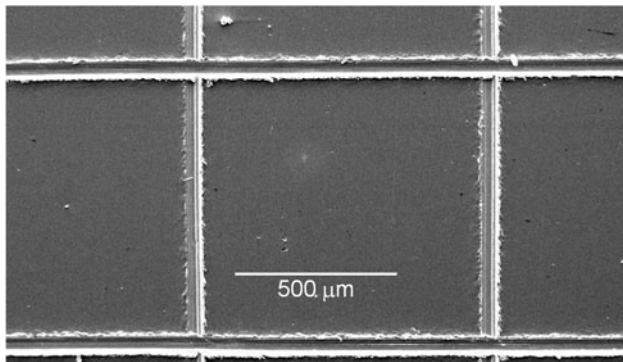


Fig. 6 Typical aspect of the surface of a stainless steel sample coated with sol-gel titania films after carrying out the cross-cut tape adhesion test

from the multiplication between the time data and the average sputter rate, their values are approximate.

One notices that the increase of the Ti signal is gradual. This confirms the presence of a lower concentration of Ti in the film surface. It is observed that the increase in the Ti content corresponds to a decrease in the oxygen profile. The film thickness was estimated by the observation of the titanium depth profile, considering the interval where the Ti intensity begins to decline and the Cr signal (first element of the substrate to be detected) acquires an expressive value. The approximate thickness of the titania film was 360 nm. According to the literature, the film thickness increases as the withdrawal speed also increases.

It is worth to point out that in the GDS experiments we have assumed that for our experiments the influence of the surface roughness on the obtained composition depth profiles is negligible. We believe that the sputtering spot used is large enough so that the effect of the surface roughness on the obtained results is not expected, especially after the substrate polishing. Furthermore, if the surface roughness were an affecting factor in the experiment, its influence could be easily detected.

3.4 Mechanical Properties

Figure 6 shows the typical aspect of the surface of stainless steel samples coated with sol-gel titania films after carrying out the cross-cut tape adhesion test. The scratches are due to the

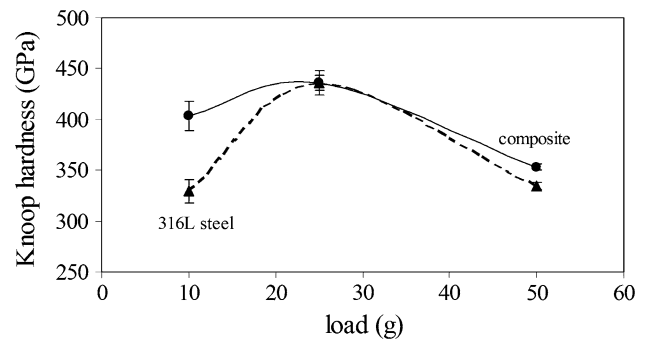


Fig. 7 Knoop hardness with the applied load for the sample heat treated at 400 °C

method used to evaluate the adherence of the film, which employs a device to produce parallel risks, spaced 1 mm from each other. The adherence of all the titania films to the stainless steel substrate was excellent, rated 5B after performing the adhesion test. The 5B adhesion rating reference in ASTM D 3359 indicates that the coating did not exhibit peeling or removal along incisions or at their intersection (Ref 26).

Static indentation tests are based on the premise that an indenter will be forced, under a predetermined load, to penetrate into the material. The hardness value is derived from the relationship between the applied load and the measured indentation depth (or area) after the test. The geometry of the Knoop indenter allows a minimal elastic recovery of the analyzed material and also makes it appropriate to measure the hardness of thin layers (Ref 38). The true or absolute value of the Knoop hardness for a thin film is obtained when the effect of the substrate material can be neglected. It means that the film thickness must be ca. 10 times greater than the indentation depth. To overcome this restriction, there is a set of indirect methods where the film and the substrate contributions can be distinguished by measuring the composite hardness (Ref 39).

Figure 7 shows the Knoop hardness values measured in two different regions of a specimen heated at 400 °C: the first one is in the bare steel at the position used to fix the specimen during the dip-coating procedure, and the second one is in the titania film/steel composite. It is observed that when loads of 25 or 50 g are used, the composite hardness is directly affected by the substrate material. Because of this we used 10 g load in our experiments.

Wang et al. (Ref 39) has developed a simple new approach for determining the film hardness from the composite hardness of the film/substrate system. This method is based on the volume law of mixtures and does not make any assumption about the mechanical properties of the analyzed material. In this work, we used the method suggested by Sargent (Ref 40). He was the first researcher to propose a model that takes into account the volume law of mixtures. Considering the volumetric fraction of the deformed region, the composite hardness can be assessed by the equation:

$$HK_{\text{composite}} = HK_{\text{film}} \cdot V_v^{\text{film}} + HK_{\text{steel}} \cdot V_v^{\text{steel}}, \quad (\text{Eq 1})$$

where $HK_{\text{composite}}$ is the composite hardness, HK_{film} is the titania film hardness, HK_{steel} is the bare steel hardness, V_v^{film} is the volumetric fraction of the indenter impression related to the film, and V_v^{steel} is the volumetric fraction related to the steel substrate. Knowing the geometry of the Knoop indenter

and measuring the diagonal length of the indentation, we are able to calculate the total volume of the impression ($V_{\text{composite}}$) by using the equation:

$$V_{\text{composite}} = V_{\text{v}}^{\text{film}} + V_{\text{v}}^{\text{steel}} = 1. \quad (\text{Eq 2})$$

Thus, we evaluated the total penetration depth by using the Knoop geometry. The penetrated fraction in the steel substrate is the difference between the total penetration depth and the film thickness. Using this value and taking into account the geometry of the Knoop indenter, $V_{\text{v}}^{\text{steel}}$ is calculated. Finally, by applying Eq 1, $V_{\text{v}}^{\text{film}}$ is obtained.

Figure 8 shows the measured hardness values as a function of the heating temperature for the bare steel and the sol-gel titania film obtained at a withdrawal speed of 60 mm/min. At 100 °C, the composite hardness is much lower than that of the bare steel. This behavior changed when the composite was heated at 400 °C: the hardness values for the composite and for

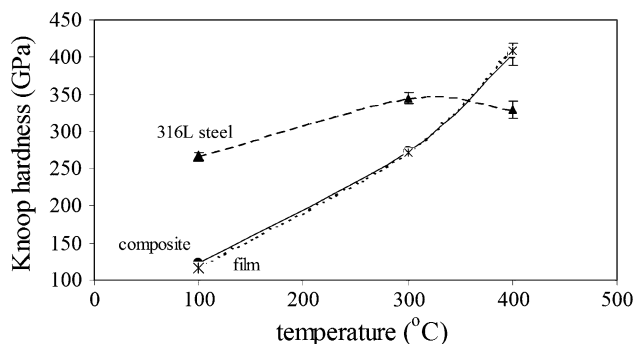


Fig. 8 HK hardness of the steel substrate, composite, and titania film. Experiments carried out using 10 g load

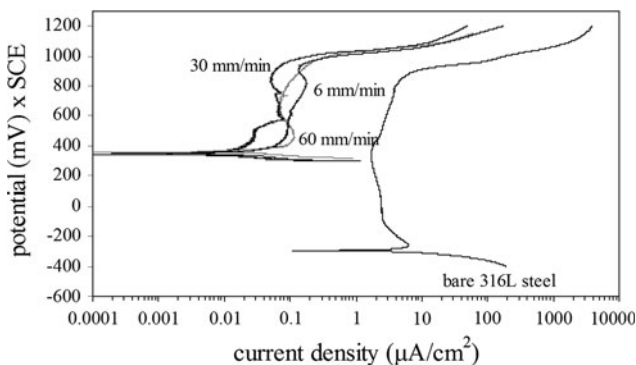


Fig. 9 Potentiodynamic polarization curves of the bare 316L steel and of the titania-coated steel at different withdrawal speeds

Table 1 Main corrosion parameters contained in Fig. 9

	Bare 316L steel	316L steel coated with sol-gel titania film		
		6 mm/min	30 mm/min	60 mm/min
Corrosion potential (E_{corr})	-295 mV	+349 mV	+346 mV	+361 mV
Corrosion current density (i_{corr})	5.64 $\mu\text{A}/\text{cm}^2$	0.015 $\mu\text{A}/\text{cm}^2$	0.013 $\mu\text{A}/\text{cm}^2$	0.016 $\mu\text{A}/\text{cm}^2$
Passivation potential (E_{pp})	-259 mV	+462 mV	+470 mV	+466 mV
Passive current density (I_{p})	2.5 $\mu\text{A}/\text{cm}^2$	0.1 $\mu\text{A}/\text{cm}^2$	0.1 $\mu\text{A}/\text{cm}^2$	0.1 $\mu\text{A}/\text{cm}^2$
Transpassivation potential (E_{t})	+821 mV	+900 mV	+905 mV	+910 mV
Corrosion rate	0.065 mm/year	0.0002 mm/yr	0.0002 mm/yr	0.0002 mm/yr

the film did not differ significantly from each other, indicating a small influence of the steel substrate.

As we expected, the composite hardness showed intermediate values between those of the substrate and the sol-gel titania film (see Fig. 8b). We observed that the titania film heated at 400 °C showed a higher hardness than the steel.

In order to measure the dispersion of the hardness data obtained, we used the variation coefficient C_v . This parameter is given by:

$$C_v = \frac{\sigma}{\bar{X}}, \quad (\text{Eq 3})$$

where σ is the standard deviation of the measured values and \bar{X} is the arithmetic mean. Taking into account the hardness values evaluated for titania films treated at the same temperature as a function of the applied load, one obtains from Eq 3 a dispersion about 10%.

3.5 Corrosion Resistance

Figure 9 shows the potentiodynamic polarization curves for the bare 316L steel before and after its coating with titania. The titania film contributes to the increase of the corrosion potential in ca. 650 mV and the passivation potential in ca. 720 mV. All coated samples presented a typical passivation behavior, in which the current density decreased and maintained a low value over a wide potential range. The passivation current density of the coated samples decreased about one order of magnitude when compared to the bare steel. This result suggests that the presence of the titania film significantly increases the chemical resistance of the steel. The potential value related to the beginning of transpassivation region was increased slightly due to the titania film deposition. The corrosion parameters contained in Fig. 9 are summarized in Table 1. The corrosion rates presented in this table were estimated through the equation (Ref 41):

$$R_{\text{Corr}} = 0.0033 i_{\text{Corr}} \frac{e}{\rho_m}, \quad (\text{Eq 4})$$

where R_{Corr} represents the corrosion rate (mm/year), i_{Corr} is the current density ($\mu\text{A}/\text{cm}^2$), e is the equivalent weight of metal, and ρ_m is the metal density (g/cm^3). According to Sedriks (Ref 41), i_{Corr} can be obtained through the curve of the applied potential as a function of current density.

4. Conclusions

The titania coatings obtained were free of cracks and presented a shining vitreous surface. The thicknesses of the

films were determined as a function of the heat treatment. We observed that their thicknesses varied from 130 to 770 nm. After performing the adhesion tests, the adherence of the titania films to the stainless steel substrate was excellent, rated 5B according to ASTM 3359. By using Knoop microindentation hardness test, we observed that these titania coatings, when heat treated, tended to be harder than the steel substrate. Their presence contributed to the increase of the corrosion potential in ca. 650 mV and the passivation potential in ca. 720 mV.

In the FTIR analyses, we observed that the increase of the sample heating temperature leads to a decrease in the absorption intensities of OH groups and of organic groups with respect to Ti-O and Ti-O-Ti bonds. When obtained as unsupported films, the sol-gel titania films presented mechanical strength enough to allow them to be bent without causing film breakage. This is an important property, with potential application for coating metal parts of different shapes and sizes.

References

1. S. Hogmark, S. Jacobson, and M. Larsson, Design and Evaluation of Tribological Coatings, *Wear*, 2000, **246**(1–2), p 20–33
2. C.J. Brinker and G.W. Scherer, *Sol-Gel Science: The Physics and Chemistry of the Sol Gel Processing*, Academic Press, San Diego, 1990
3. J.D. Mackenzie and E.P. Bescher, Physical Properties of Sol-Gel Coatings, *J. Sol-Gel Sci. Technol.*, 2000, **19**(1–3), p 23–29
4. C.J. Brinker, A.J. Hurd, G.C. Frye, P.R. Schunk, and C.S. Ashley, Sol-Gel Thin-Film Formation, *Chemical Processing of Advanced Materials*, 1st ed., L.L. Hench and J.K. West, Ed., John Wiley & Sons Inc., New York, 1992, p 395
5. L.M. Sheppard, Sol-Gel: Making Its Way Into The Mainstream, *Photonics Spectra*, 2000, **34**(1), p 128–132
6. H. Ohsaki and Y. Kokubu, Global Market and Technology Trends on Coated Glass for Architectural, Automotive and Display Applications, *Thin Solid Films*, 1999, **351**(1–2), p 1–7
7. R.A. Caruso and M. Antonietti, Sol-Gel Nanocoating: An Approach to the Preparation of Structured Materials, *Chem. Mater.*, 2001, **13**(10), p 3272–3282
8. K. Abe, Y. Sanada, and T. Morimoto, Anti-Reflective Coatings for CRTs by Sol-Gel Process, *J. Sol-Gel Sci. Technol.*, 2003, **26**(1–3), p 709–713
9. M.L. Zheludkevich, R. Serra, M.F. Montemor, K.A. Yasakau, I.M. Miranda Salvado, and M.G.S. Ferreira, Nanostructured Sol-Gel Coatings Doped with Cerium Nitrate as Pre-Treatments for AA2024-T3 Corrosion Protection Performance, *Electrochim. Acta*, 2005, **51**(2), p 208–217
10. A.N. Khranov, V.N. Balbyshev, L.S. Kasten, and R.A. Mantz, Sol-Gel Coatings with Phosphonate Functionalities for Surface Modification of Magnesium Alloys, *Thin Solid Films*, 2006, **514**(1–2), p 174–181
11. D.C.L. Vasconcelos, R.L. Oréfice, and W.L. Vasconcelos, Processing of Sol-Gel Alumina Coatings on Stainless Steel Substrates, *Acta Microsc.*, 1999, **8**(Supplement A), p 321–322
12. O. Sanctis, L. Gómez, N. Pellegrini, and A. Durán, Behaviour in Hot Ammonia Atmosphere of SiO₂-Coated Stainless Steels Produced by a Sol-Gel Procedure, *Surf. Coat. Technol.*, 1995, **70**(2–3), p 251–255
13. F.T. Cheng, P. Shi, and H.C. Man, Anatase Coating on NiTi via a Low-Temperature Sol-Gel Route for Improving Corrosion Resistance, *Scr. Mater.*, 2004, **51**(11), p 1041–1045
14. M.L. Zheludkevich, I.M. Salvado, and M.G.S. Ferreira, Sol-Gel Coatings for Corrosion Protection of Metals, *J. Mater. Chem.*, 2005, **15**(48), p 5099–5111
15. K.Y. Chiu, M.H. Wong, F.T. Cheng, and H.C. Man, Characterization and Corrosion Studies of Titania-Coated NiTi Prepared by Sol-Gel Technique and Steam Crystallization, *Appl. Surf. Sci.*, 2007, **253**(16), p 6762–6768
16. H. Hasannejad, M. Aliofkhazraei, A. Shanaghi, T. Shahrabi, and A.R. Sabour, Nanostructural and Electrochemical Characteristics of Cerium Oxide Thin Films Deposited on AA5083-H321 Aluminum Alloy Substrates by Dip Immersion and Sol-Gel Methods, *Thin Solid Films*, 2009, **517**(17), p 4792–4799
17. G. Grundmeier, W. Schmidt, and M. Stratmann, Corrosion Protection by Organic Coatings: Electrochemical Mechanism and Novel Methods of Investigation, *Electrochim. Acta*, 2000, **45**(15–16), p 2515–2533
18. S. de Souza, J.E.P. da Silva, S.I.C. de Torresi, M.L.A. Temperini, and R.M. Torresi, Polyaniline Based Acrylic Blends for Iron Corrosion Protection, *Electrochem. Solid-State Lett.*, 2001, **4**(8), p B27–B30
19. H. Cao, R. Zhang, C.S. Sundar, J.-P. Yuan, Y. He, T.C. Sandreczki, Y.C. Jean, and B. Nielsen, Degradation of Polymer Coating Systems Studied by Positron Annihilation Spectroscopy: 1. UV Irradiation Effect, *Macromolecules*, 1998, **31**, p 6627–6635
20. A. Miszczyk and K. Darowicki, Effect of Environmental Temperature Variations on Protective Properties of Organic Coatings, *Prog. Org. Coat.*, 2003, **46**(1), p 49–54
21. D.C.L. Vasconcelos, “Non-Oriented Grain Silicon Steel/Stainless Steel Composites Coated with Magnesia, Alumina, Silica and Titania Films Prepared by Sol-Gel,” PhD Thesis, Federal University of Minas Gerais, 2003 (in Portuguese)
22. K. Izumi, N. Minami, and Y. Uchida, Sol-Gel Derived Coatings on Steel Sheets, *Key Eng. Mater.*, 1998, **150**, p 77–87
23. D.C.L. Vasconcelos, J.A.N. Carvalho, M. Mantel, and W.L. Vasconcelos, Corrosion Resistance of Stainless Steel Coated with Sol-Gel Silica, *J. Non-Cryst. Solids*, 2000, **273**(1–3), p 135–139
24. M. Atik, S.H. Messaddeq, F.P. Luna, and M.A. Aegerter, Zirconia Sol-Gel Coatings Deposited on 304 and 316L Stainless Steel for Chemical Protection in Acid Media, *J. Mater. Sci. Lett.*, 1996, **15**(23), p 2051–2054
25. Y. Takahashi and Y. Matsuoka, Dip-Coating of TiO₂ Films Using a Sol Derived From Ti(O-I-PR)₄-Diethanolamine-H₂O-I-Proh System, *J. Mater. Sci.*, 1988, **23**(6), p 2259–2266
26. “Standard Test Methods for Measuring Adhesion by Tape Test,” D3359, Annual Book of ASTM Standards, ASTM International, p 1–7
27. S. Musić, M. Gotić, M. Ivanda, S. Popović, A. Turković, R. Trojko, A. Sekulić, and K. Furić, Chemical and Microstructural Properties of TiO₂ Synthesized by Sol-Gel Procedure, *Mater. Sci. Eng. B*, 1997, **47**, p 33–40
28. C. Suresh, V. Biju, P. Mukundan, and K.G.K. Warriar, Anatase to Rutile Transformation in Sol-Gel Titania by Modification of Precursor, *Polyhedron*, 1998, **17**(18), p 3131–3135
29. S.R. Kumar, C. Suresh, A.K. Vasudevan, N.R. Sujana, P. Mukundan, and K.G.K. Warriar, Phase Transformation in Sol-Gel Titania Containing Silica, *Mater. Lett.*, 1999, **38**(3), p 161–166
30. T. Lopez, E. Sanchez, P. Bosch, Y. Meas, and R. Gomez, FTIR and UV-VIS (Diffuse Reflectance) Spectroscopic Characterization of TiO₂ Sol-Gel, *Mater. Chem. Phys.*, 1992, **32**(2), p 141–152
31. K. Chhor, J.F. Bocquet, and C. Pommier, Syntheses of Submicron TiO₂ Powders in Vapor, Liquid and Supercritical Phases: A Comparative-Study, *Mater. Chem. Phys.*, 1992, **32**(3), p 249–254
32. D.L. Wood, E.M. Rabinovich, D.W. Johnson, Jr., J.B. MacChesney, and E.M. Vogel, Preparation of High-Silica Glasses From Colloidal Gels. 3. Infrared Spectrophotometric Studies, *J. Am. Ceram. Soc.*, 1983, **66**(10), p 693–699
33. M. Burgos and M. Langlet, The Sol-Gel Transformation of TIPT Coatings: A FTIR Study, *Thin Solid Films*, 1999, **349**(1–2), p 19–23
34. R. Urlaub, U. Posset, and R. Thull, FT-IR Spectroscopic Investigations on Sol-Gel-Derived Coatings from Acid-Modified Titanium Alkoxides, *J. Non-Cryst. Solids*, 2000, **265**(3), p 276–284
35. S. Doeuff, M. Henry, C. Sanchez, and J. Livage, Hydrolysis of Titanium Alkoxides: Modification of the Molecular Precursor by Acetic Acid, *J. Non-Cryst. Solids*, 1987, **89**(1–2), p 206–216
36. P.A. Venz, R.L. Frost, and J.T. Klopogge, Chemical Properties of Modified Titania Hydrolysates, *J. Non-Cryst. Solids*, 2000, **276**(1–3), p 95–112
37. F.N. Castellano, J.M. Stipkala, L.A. Friedman, and G.L. Meyer, Spectroscopic and Excited-State Properties of Titanium-Dioxide Gels, *Chem. Mater.*, 1994, **6**, p 2123–2129
38. G.F.V. Voort and G.L. Buehler, Microindentation Hardness Testing, U.S.A., 09/11/2000, <http://www.metallography.com/amp/micro.html>

39. H.L. Wang, M.J. Chiang, and M.H. Hon, Determination of Thin Film Hardness for a Film/Substrate System, *Ceram. Int.*, 2001, **27**(4), p 385–389
40. P.M. Sargent, Use of the Indentation Size Effect on Microhardness for Materials Characterization, *Microindentation Techniques in Materials Science and Engineering*, P.L. Blau and B.R. Lawn, Ed., ASTM Special Technical Publication, Philadelphia, 1985, p 160
41. A.J. Sedriks, *Corrosion of Stainless Steels*, 2nd ed., Wiley-Interscience, New York, 1996, p 464